Report

Current Biology

Progressive Decrease of Mitochondrial Motility during Maturation of Cortical Axons In Vitro and In Vivo

Highlights

- Mitochondrial motility is greatly reduced during cortical axon maturation in vitro
- Mitochondrial immobilization correlates with their capture at presynaptic boutons
- Axonal mitochondria remain immobilized over long time periods in mature neurons
- Mitochondrial motility is very limited in adult cortical axons in vivo

Authors

Tommy L. Lewis, Jr., Gergely F. Turi, Seok-Kyu Kwon, Attila Losonczy, Franck Polleux

Correspondence

fp2304@cumc.columbia.edu

In Brief

Lewis et al. demonstrate that mitochondrial motility is extremely low in mature cortical axons in vitro and in vivo using two-photon microscopy in awake-behaving mice. These results establish that the identification of the molecular mechanisms underlying mitochondrial immobilization at specific points along the axon is becoming critical.

Lewis et al., 2016, Current Biology *26*, 1–7
October 10, 2016
http://dx.doi.org/10.1016/j.cub.2016.07.064

CellPress

Please cite this article in press as: Lewis et al., Progressive Decrease of Mitochondrial Motility during Maturation of Cortical Axons In Vitro and In Vivo, Current Biology (2016), http://dx.doi.org/10.1016/j.cub.2016.07.064

Current Biology
Report

Progressive Decrease of Mitochondrial Motility during Maturation of Cortical Axons In Vitro and In Vivo

Tommy L. Lewis, Jr.,[1] Gergely F. Turi,[1] Seok-Kyu Kwon,[1] Attila Losonczy,[1] and Franck Polleux[1,2,*]
[1]Department of Neuroscience, Columbia University Medical Center, Mortimer B. Zuckerman Mind Brain Behavior Institute, Kavli Institute for Brain Science, 550 West 120th Street, 1103 NWC Building, New York, NY 10027, USA
[2]Lead Contact
*Correspondence: fp2304@cumc.columbia.edu
http://dx.doi.org/10.1016/j.cub.2016.07.064

SUMMARY

The importance of mitochondria for neuronal function is evident by the large number of neurodegenerative diseases that have been associated with a disruption of mitochondrial function or transport (reviewed in [1, 2]). Mitochondria are essential for proper biological function as a result of their ability to produce ATP through oxidative phosphorylation, buffer cytoplasmic calcium, regulate lipid biosynthesis, and trigger apoptosis (reviewed in [2]). Efficient transport of mitochondria is thought to be particularly important in neurons in light of their compartmentalization, length of axonal processes, and high-energy requirements (reviewed in [3]). However, the majority of these results were obtained using short-term, in vitro neuronal culture models, and very little is currently known about mitochondrial dynamics in mature axons of the mammalian CNS in vitro or in vivo. Furthermore, recent evidence has demonstrated that mitochondrial immobilization at specific points along the axon, such as presynaptic boutons, play critical roles in axon morphogenesis [4, 5]. We report that as cortical axons mature, motility of mitochondria (but not other cargoes) is dramatically reduced and this coincides with increased localization to presynaptic sites. We also demonstrate using photo-conversion that in vitro mature axons display surprisingly limited long-range mitochondrial transport. Finally, using in vivo two-photon microscopy in anesthetized or awake-behaving mice, we document for the first time that mitochondrial motility is also remarkably low in distal cortical axons in vivo. These results argue that mitochondrial immobilization and presynaptic localization are important hallmarks of mature CNS axons both in vitro and in vivo.

RESULTS AND DISCUSSION

Mitochondrial Motility Decreases Progressively with Axonal Maturation and Coincides with Increased Presynaptic Localization In Vitro

To better understand mitochondrial localization at presynaptic sites, we performed live dual-channel time-lapse imaging of mitochondria and VGLUT1-labeled presynaptic boutons following ex utero cortical electroporation, dissociation, and primary neuronal culture. As previously observed, early stages (3–7 days in vitro [DIV]) of axonal development display a substantial fraction of highly motile mitochondria (Figures 1A and 1B) [4, 6, 7]. However, as the axon matured ($\geq$10 DIV), mitochondria became less motile (Figures 1C–1G and 1I). By 28 DIV, more than 95% of axonal mitochondria were stationary over the 30 min of imaging compared to ~60% at 7 DIV (ANOVA, $p < 0.0001$). This decrease in mitochondrial motility coincides with the formation of stable en passant VGLUT1-positive presynaptic sites along the axon (Figures 1B–1F; Movie S1). Stable presynaptic boutons begin to appear around 7 DIV, thus we quantified the percent of stationary mitochondria localized at stable presynaptic sites for the entire 30 min of imaging (Figures 1H and 1I) and found that early in axonal development (7 DIV) ~20% of stationary mitochondria are localized at presynaptic sites. This percentage steadily increases with development until approximately half of all axonal mitochondria are localized at presynaptic boutons (Figure 1H; ANOVA, $p < 0.0001$). Interestingly, this represents a substantial increase in presynaptic localization when one considers that ~40% of mitochondria at 7 DIV are not included in this quantification as they are not stationary. Our data so far suggests a model whereby mitochondrial motility is significantly lower in mature axons than previously proposed from the results obtained in immature, developing axons of dissociated cultured neurons (usually 5–7 DIV; e.g., [8, 9]). In the present report and another recent study in hippocampal neurons [10], mitochondria are shown to be considerably more stable in mature axons ($\geq$14 DIV) than in immature axons in vitro. These reports also demonstrate that mitochondrial immobilization correlates with their localization to presynaptic boutons along CNS axons (Table S1). Together, these results reveal that mitochondrial motility decreases with axonal maturation partially as a result of presynaptic immobilization. In the future, it will be important to better understand the cellular and molecular mechanisms that regulate

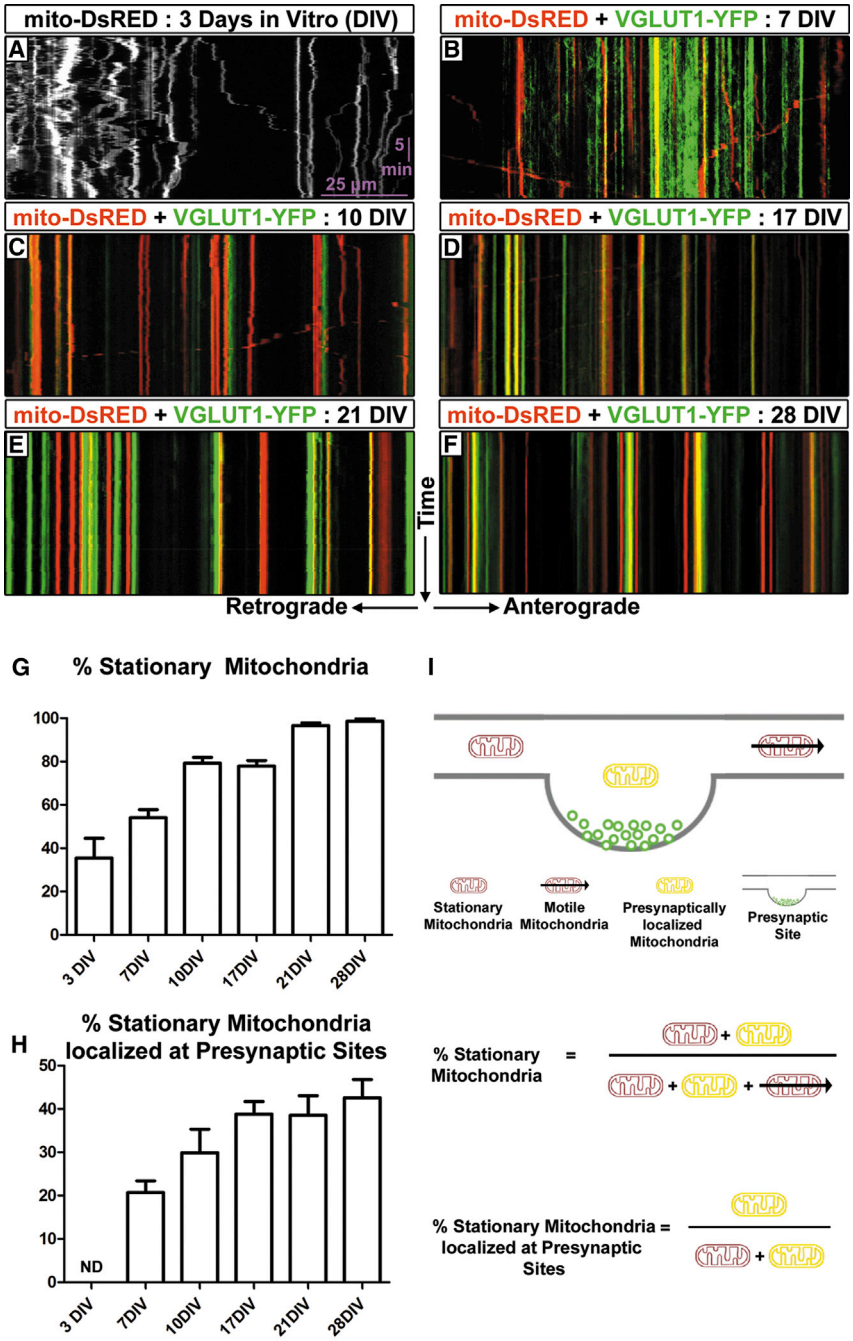

Figure 1. Mitochondrial Motility Decreases as the Axon Matures In Vitro

(A) Representative kymograph of mitochondria in the axon of a cultured cortical neuron at 3 DIV. On average, only 35% of mitochondria are stationary. Stationary mitochondria are those mitochondria that move <5 μm from the point of origin over the 30 min of time-lapse microscopy. The y axis represents time, and the x axis represents direction of transport. Time-lapse videos were acquired at 0.1 frames per second (fps) for 30 min.

(B–F) Representative dual color kymographs of mitochondria (red) and VGLUT1 (green) in the axons of cultured cortical neurons at 7 DIV (B), 10 DIV (C), 17 DIV (D), 21 DIV (E), and 28 DIV (F).

(G) Graph demonstrating the percent of stationary axonal mitochondria at various days in culture. Axonal development coincides with an increase in the number of stationary mitochondria.

(H) Graph demonstrating the percent of stationary mitochondria that are localized at presynaptic sites. Localization is defined as overlap with the same stationary VGLUT1 puncta for the entire 30 min of the time lapse. The decrease in axonal mitochondrial motility coincides with increased localization of mitochondria at presynaptic sites.

(I) Schematic representation of the parameters calculated in (G) and (H).

n = 8, 27, 15, 17, 17, and 18 axon segments at 3, 7, 10, 17, 21, and 28 DIV, respectively. Statistical test: ANOVA with Dunn's multiple-comparison test. All error bars represent the SEM. See also Figure S1, Table S1, and Movie S1.

long-term immobilization of mitochondria, the role of mitochondria localized at presynaptic sites versus other sites along the axon, as well as the effects that presynaptically localized mitochondria exert on presynaptic release properties.

Lysosomal Motility Is Not Affected by Axonal Maturation In Vitro

To determine whether the decrease in mitochondrial motility is specific to this cargo or whether cargo trafficking in general is lower in mature axons, we performed live dual-channel time-lapse imaging of LAMP1-labeled lysosomes and mitochondria in immature (7 DIV) and mature (28 DIV) axons (Figures 2A–2F; Movie S2). We chose lysosomes as a cargo because recent evidence suggested that axonal mitochondria are locally engaged by autophagosomes fusing to lysosomes for removal by local mitophagy [11, 12]. While the fraction of stationary mitochondria increases from ~65% to ~98% between 7 DIV and 28 DIV, the percentage of stationary lysosomes did not change significantly (Figure 2G; ANOVA, $p < 0.05$ for mitochondria, no significance for lysosomes). While the number of motile versus stationary lysosomes was not changed, there was a decrease in the velocity of the lysosomes and a small increase in retrograde run time in mature axons (Figure 2H; ANOVA, $p < 0.001$ for velocity, $p < 0.05$ for retrograde run time). The observation that the fraction of motile lysosomes is unchanged in mature axons is consistent with recent work demonstrating that autophagosomes need to be transported back to the cell body to undergo fusion with lysosomes [13] and suggests that the decrease in mitochondrial motility in mature axons in vitro is rather specific to this organelle.

Mitochondria in Mature Axons Are Functional

One possible explanation for the decrease in mitochondrial motility observed in late stage cultures could be that mitochondrial

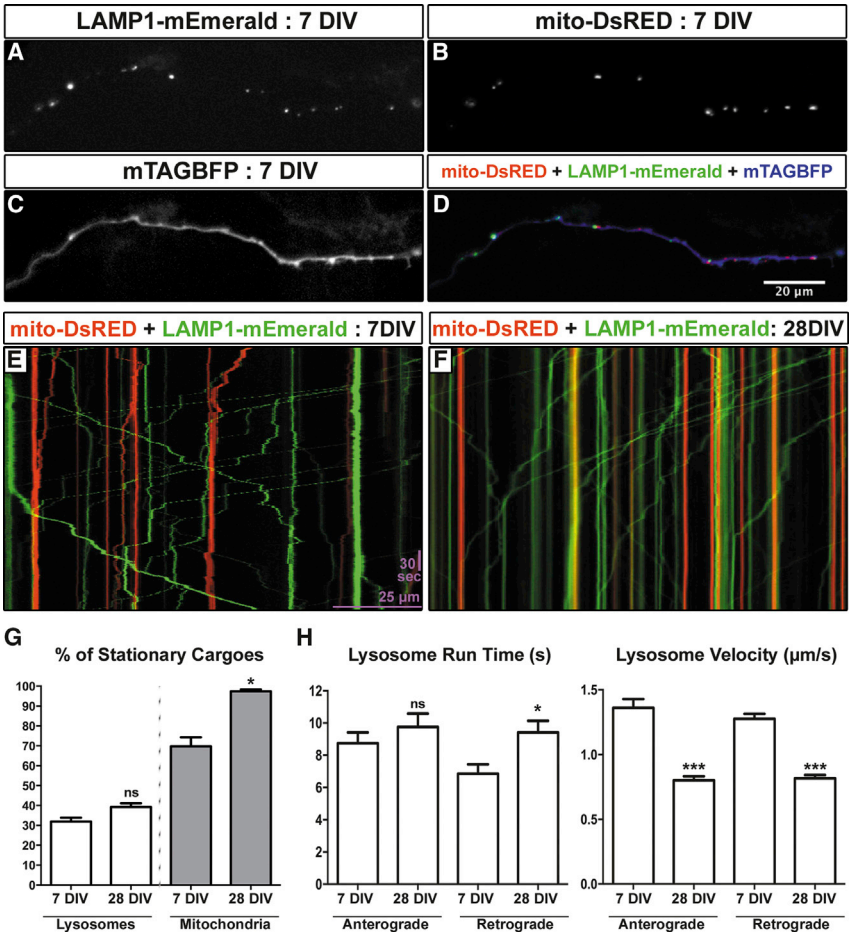

Figure 2. Lysosome Motility Does Not Decrease during Axonal Maturation In Vitro

(A–D) Representative images of a 7 DIV axon expressing LAMP1-mEmerald (A), mitoDsRED (B), and mTAGBFP (C) after ex utero electroporation at E15.5. A merge of (A) (green), (B) (red), and (C) (blue) is shown in (D).

(E) Representative kymograph of mitochondria (red) and LAMP1 (green) in the axon of a cultured cortical neuron at 7 DIV. Kymograph axes are the same as in Figure 1.

(F) Representative kymograph of mitochondria (red) and LAMP1 (green) in the axon of a cultured cortical neuron at 28 DIV.

(G) Graph comparing the percent of stationary lysosomes to the percent of stationary mitochondria at 7 and 28 DIV. The number of motile axonal lysosomes doesn't change significantly between 7 and 28 DIV, while the percentage of stationary axonal mitochondria increases at 28 DIV.

(H) Graphs comparing lysosomal run time and velocity of anterograde and retrograde transport at 7 and 28 DIV. While run time slightly increases for motile lysosomes, the velocity is much less at 28 DIV. n = 18 axon segments at 7 DIV and 26 axon segments at 28 DIV. Statistical test: ANOVA with Dunn's multiple-comparison test. All error bars represent the SEM. See also Movie S2.

function is compromised. To measure the functionality of mitochondria under these conditions, we imaged mitochondrial membrane potential via tetramethylrhodamine (TMRM) [14], and mitochondrial matrix calcium dynamics during action potential (AP) evoked neurotransmitter release using a genetically encoded, matrix-targeted calcium indicator GCaMP5G (mito-GCaMP5G) [15]. Mitochondrial membrane potential is generated via the proton gradient, resulting from oxidative phosphorylation along the electron transport chain (ETC), across the inner mitochondrial membrane (IMM) that gates ATP generation. We observed that mitochondria in the axon of neurons cultured for 7 DIV or 28 DIV effectively took up TMRM and determined that there was no difference in the ratio of mitochondrial fluorescence to cytoplasmic fluorescence (Fm/Fc) [14] (Figures S1A and S1B). This result establishes that mitochondria do not display significant changes in their membrane potential during axon maturation in vitro. To test whether or not mitochondria are capable of importing calcium during AP-evoked release [16], we applied 100APs at 10 Hz using a microelectrode stimulation near the labeled axons and found that mitochondria in both immature and mature axons responded by importing calcium into their matrix on similar timescales (Figures S1D–S1G). We calculated the area under the curves (as an estimate of the "total charge transfer") and found a small but significant increase in the amount of calcium imported by mitochondria in mature axons in vitro (Figure S1G). We also observed an increase in the basal level of calcium in the matrix of mitochondria in mature axons compared to immature axons (Figure S1E). It is likely that increased neuronal activity, mediated by mature synapses, in these older cultures is at least partially responsible for both the increased basal level of calcium in the mitochondrial matrix and the increase in calcium that is imported upon stimulation. This increase in AP-evoked mitochondrial calcium import in mature axons might be linked to decreased mitochondrial motility, although the mechanisms by which intramitochondrial calcium regulate mitochondrial trafficking remain controversial [8, 17–19].

Long-Term Time-Lapse Microscopy Reveals that Mitochondria in Mature Axons Remain Stable over an Extended Period of Time

To determine the stability of mitochondria over a more extended period of time, we used photo-convertible mEos2 [20, 21] targeted to the mitochondrial matrix (mito-mEos2) (Figures 3A and 3B). This allowed us to label a few mitochondria in distal portions of the axon and image at a much lower frequency (once every 15 min) for a longer period of time (12 hr) yet still determine unambiguously that the same mitochondria are present over extended periods of time. Semi-automated tracking of the photo-converted mitochondria (Figures 3C and 3D) revealed that 75% of mitochondria remained within 10 µm of their original position over 12 hr, thus demonstrating that most mitochondria remain immobile over long periods of time in mature cortical axons in vitro (Figure 3E; Movie S3).

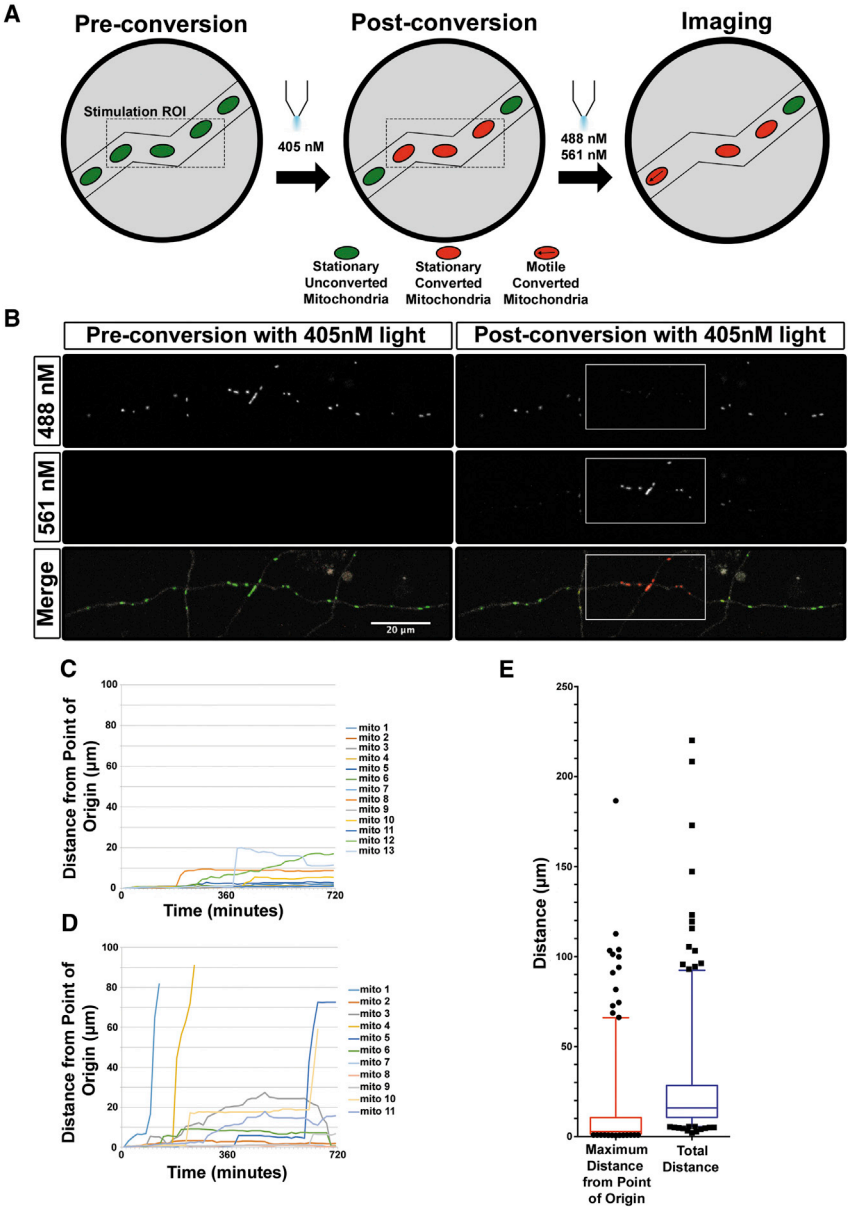

Figure 3. Long-Term Time-Lapse Microscopy with Photo-Convertible mEos2 Reveals Highly Stable Mitochondria in Mature Axons In Vitro

(A) Schematic representation of long-term time-lapse imaging setup. Upon photo-conversion of mito-mEos2, all mitochondria within a short segment of the axon (30–50 μm) were converted from green to red fluorescence. Time-lapse imaging was then performed every 15 min for 12 hr for both the red and green forms of mEos2.

(B) A 28 DIV cortical axon expressing mito-mEos2 before and after photo-conversion by 405 nm light. White boxes label the ROI for 405 nm stimulation.

(C) Graph of individual photo-converted mitochondrial motility in a representative axon with low mitochondrial motility.

(D) Graph of individual photo-converted mitochondrial motility in an axon with higher mitochondrial motility.

(E) Quantification of maximum distance from the point of origin and total distance moved for each mitochondria tracked over 12 hr revealing that 75% of mitochondria moved 10 μm or less from their original positions. n = 261 mitochondria from 23 axons (four independent cultures). Data are represented as 5%–95% whisker box plots with 25th, 50th, and 75th percentiles shown by the lower, middle, and top of the boxes. Outliers are represented by black dots.

See also Movie S3.

Mitochondrial Motility Is Low in Distal Layer 2/3 Axons In Vivo

Finally, we wanted to determine whether the results we had obtained in mature cortical axons in vitro were recapitulated in vivo where the environment is much more complex than in a culture dish and obviously more physiological regarding metabolism, cell type diversity, and cellular architecture [22, 23]. To do this, we implemented an imaging paradigm for visualizing mitochondrial motility in distal layer 2/3 axons of cortical pyramidal neurons by in vivo two-photon microscopy (Figure 4A). In short, mouse embryos were electroporated unilaterally in utero at embryonic day E15.5 (to target progenitors giving rise to layer 2/3 pyramidal neurons) with plasmids encoding mito-YFP and cytosolic tdTomato. Postnatal (P) day 10–12 or P23–P24 mice were fitted with a cranial window and a head-fixing post for live imaging on a two-photon microscope [24]. As shown in Figure 4B, we were able to find and image distal layer 2/3 axons filled with labeled mitochondria and tdTomato on the side contralateral to the electroporated hemisphere. We first performed live imaging on anesthetized mice at P10–P12 and P29–P30 (Figure 4C). Surprisingly even at the early developmental stage of P10–P12, mitochondria are highly immobile with ~90% of mitochondria being stable for the entire imaging session (10–20 min; Figures 4D and 4E). Because different forms of anesthesia are known to affect mitochondrial function, and therefore may affect mitochondrial dynamics [25–28], we performed imaging on awake behaving mice at P30–P33 and P45 to demonstrate that anesthesia was not the reason for the lack of mitochondrial motility, (Figure 4C; Movie S4) and established again that >90% of mitochondria were stationary over the entire imaging session (Figures 4D and 4E; ANOVA, p = 0.1097). Recent advances in imaging and surgical techniques have begun to allow for the study of mitochondrial motility and function in vivo. Misgeld et al. provided the first hint that mitochondrial motility is likely to be low in vivo when they showed in the sciatic nerve (peripheral nervous system [PNS]) of mice that ~90% of mitochondria are stationary both in slice preparations and in vivo [29]. In Rohon-Beard cells (PNS) of zebrafish, in vivo imaging of axonal mitochondria revealed a low percentage of moving mitochondria (between 1%–17%) that depended on the distance of the imaged segment from the cell body [30].

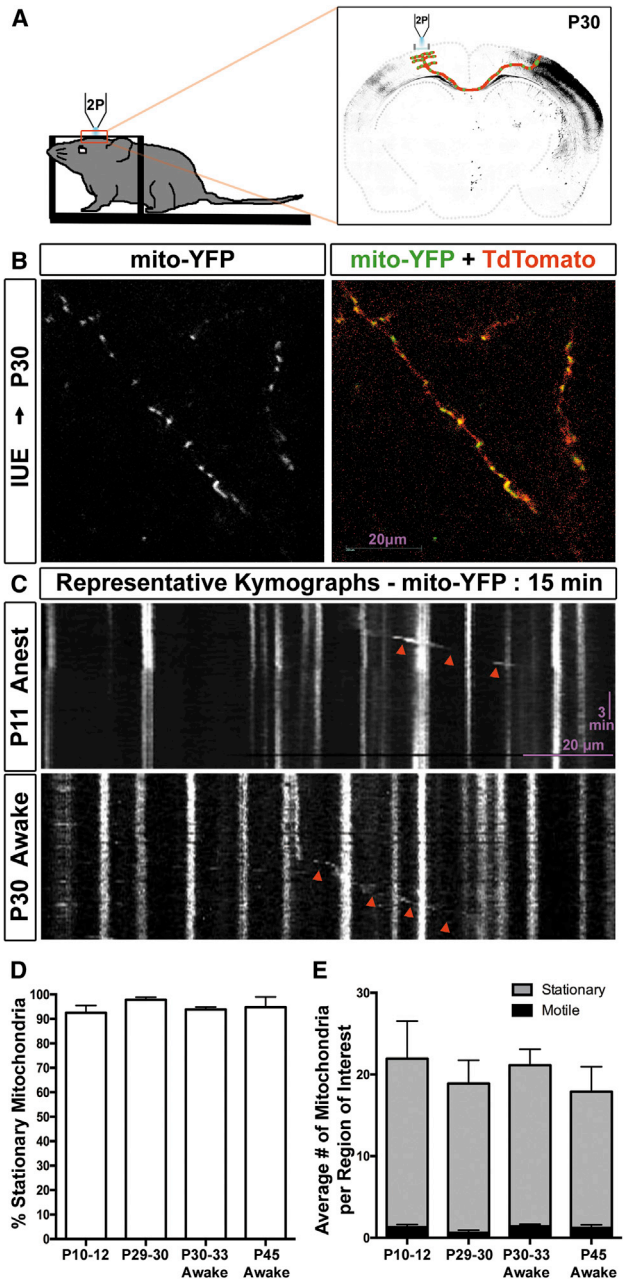

Figure 4. Mitochondrial Motility Is Remarkably Low in Distal Layer 2/3 Axons In Vivo

(A) Schematic representation of the imaging setup used to image axonal mitochondria in layer 2/3 pyramidal axon collaterals via two-photon microscopy after in utero electroporation at E15.5.

(B) Representative imaging field from the contralateral hemisphere at postnatal day 30. Left: mitochondria labeled with YFP. Right: merge of mito-YFP and tdTomato to visualize the axon collaterals.

(C) Representative kymographs of mitochondria labeled with YFP and imaged over a period of 15 min at 0.1 fps. Top: mitochondrial motility at P11. Bottom: mitochondrial motility at P30. Red arrowheads point to motile mitochondria.

(D) Graph demonstrating the percent of stationary mitochondria under four different conditions: P10–P12 anesthetized mice, P29–P30 anesthetized mice, P30–P33 awake mice, and P45 awake mice. Mitochondrial motility is remarkably low in all four conditions.

(E) Graph comparing the number of motile and stationary mitochondria in the four conditions tested. n = 17, 11, 24, and 9 regions of interest from six, three, six, and two mice at P10–P12 (anesthetized), P29–P30 (anesthetized), P30–P33 (awake), and P45 (awake), respectively.

Statistical test: ANOVA with Dunn's multiple-comparison test. All error bars represent the SEM. See also Movie S4.

Finally, imaging of mitochondrial dynamics in mouse PNS axons of the saphenous nerves also revealed a high percentage of stationary mitochondria in vivo but found that high levels of neuronal activity significantly increased anterograde transport of mitochondria [31]. Coupled with other reports, our present results examining mammalian CNS cortical axons indicate that mitochondrial motility must be examined in mature in vitro and in vivo axons rather than immature in vitro culture models for inference of the molecular and cellular mechanisms underlying mitochondria dynamics and function in neurodegenerative diseases [32] (Table S1). An interesting example of this is with the mitochondrial anchoring protein syntaphilin (SNPH). Loss of SNPH in short-term cultures from knockout mice show a dramatic increase in the number of motile mitochondria, but in slice cultures from 4-month-old knockout mice the number of motile mitochondria is still very low, suggesting that other mechanisms for capturing/stabilizing mitochondria must be present [33, 34].

A recent report showing that mitochondrial transport is highly dynamic in axons of retinal ganglion cells in vivo [35] proposed that other current forms of imaging are too invasive and claim this is the reason for the low motility that is seen by other groups. However, based on multiple recent reports using different axon subtypes and procedures [29–32, 34, 36, 37] (see Table S1), and also based on our present report showing that 21 days after window implantation mitochondrial motility is still very low in cortical axons of adult awake behaving mice, it is unlikely that inflammation or surgical procedure is the reason for these results. We believe that this discrepancy could be the result of a few different factors: (1) as mentioned above, distance from the cell body most likely plays a role in the motility profile of the imaged mitochondria [30, 38], (2) based on this work and others, the motility profile is most likely also influenced by the presence or absence of anchoring sites such as synaptic boutons and Nodes of Ranvier or in portions of the axons that are myelinated [10, 34], and (3) it is likely that different types of neurons will have different motility profiles when considering the vast array of activity profiles that are found in vivo [10, 31, 34].

Finally, it is interesting to note that in dendrites of retinal ganglion cells examined in whole mount preparations, mitochondrial motility is also reduced as the neuron matures (~70% stationary mitochondria at P9 versus ~100% at P21) [37]. These authors nicely demonstrate that this is mitochondria-specific (e.g., peroxisomes do not show this decreased in motility in adult stages) and that neither spontaneous nor sensory-evoked activity patterns regulate mitochondria dynamics.

Much of the literature examining mitochondrial dynamics in CNS axons has focused on the molecular mechanisms underlying their transport through microtubule-based motors such as dyneins and kinesins. Our results strongly argue that in the future, it will be important to improve our understanding of the

mechanisms regulating mitochondrial immobilization, as well as the role that stationary mitochondria play at specific points along the axon. It is imperative that we devise the tools necessary to study mitochondria dynamics and function in vivo, in awake adult mice, over extended periods of time.

EXPERIMENTAL PROCEDURES

Animals

All animals were handled according to protocols approved by the Institutional Animal Care and Use Committee (IACUC) at Columbia University. Time-pregnant CD1 females were purchased from Charles Rivers. Timed-pregnant hybrid F1 females were obtained by mating inbred 129/SvJ females and C57Bl/6J males in house [4].

In Utero Cortical Electroporation

In utero electroporations were performed as detailed in [4] with the exception that CD1 mice were used. See the Supplemental Experimental Procedures for more details.

Primary Cortical Culture and Ex Utero Electroporation

Cortices from E15.5 CD1 mouse embryos were dissected followed by dissociation in complete Hank's balanced salt solution (cHBSS) containing papain (Worthington) and DNase I (100 μg/mL, Sigma) for 20 min at 37°C, washed three times, and manually triturated in cHBSS supplemented with DNase. Cells were plated at 7.5×10^4 cells per 35 mm glass bottom dish (Mattek) coated with poly-D-lysine (1 mg/mL, Sigma) and cultured for 3–28 days in neurobasal medium supplemented with B27 (1×), FBS (2.5%), L-glutamine (2 mM). One-third of the medium was changed every 5 days thereafter with non-FBS containing medium. Ex utero electroporation was performed as previously published in [4]. See the Supplemental Experimental Procedures for details and constructs.

Imaging

Imaging on dissociated neurons was performed between 3–28 DIV on a Nikon Ti-e with either an EM-CCD camera (Andor) or A1 confocal (Nikon). All in vivo imaging was performed on a custom two-photon microscope (Bruker) in resonant galvo-mode and an ultra-fast pulsed laser tuned to 920 nm (Coherent). See the Supplemental Experimental Procedures for detailed imaging methods.

SUPPLEMENTAL INFORMATION

Supplemental Information includes Supplemental Experimental Procedures, one figure, one table, and four movies and can be found with this article online at http://dx.doi.org/10.1016/j.cub.2016.07.064.

AUTHORS CONTRIBUTIONS

T.L. performed cranial window surgeries, in vivo two-photon imaging, ex utero and in utero cortical electroporation, dissociated cultures, time lapse imaging, and analyzed the results and wrote the manuscript. G.T. performed cranial window surgeries, in vivo two-photon imaging, in vivo image registration, and wrote the manuscript. S.K. performed mito-GCAMP imaging, analysis, and wrote the manuscript. A.L. oversaw all in vivo two-photon imaging experiments and wrote the manuscript. F.P. conceived and oversaw all experiments and analysis and wrote the manuscript.

ACKNOWLEDGMENTS

Funding sources include NIH-R01NS089456-08 (F.P.), NIH-F32NS080464 (T.L.), NIH-K99NS091526 (T.L.), Human Frontiers Science Program Long-term Fellowship (S.K.), Human Frontiers Science Program (A.L.) and McKnight Foundation (A.L.), and the Kavli Institute for Brain Science at Columbia University (F.P., A.L.). The authors would like to thank members of the F.P. and A.L. labs for helpful suggestions, technical advice, and critical reading of the manuscript.

Received: January 5, 2016
Revised: July 21, 2016
Accepted: July 26, 2016
Published: September 15, 2016

REFERENCES

1. Chen, H., and Chan, D.C. (2009). Mitochondrial dynamics–fusion, fission, movement, and mitophagy–in neurodegenerative diseases. Hum. Mol. Genet. *18* (R2), R169–R176.
2. Schon, E.A., and Przedborski, S. (2011). Mitochondria: the next (neurode) generation. Neuron *70*, 1033–1053.
3. Hirokawa, N., Niwa, S., and Tanaka, Y. (2010). Molecular motors in neurons: transport mechanisms and roles in brain function, development, and disease. Neuron *68*, 610–638.
4. Courchet, J., Lewis, T.L., Jr., Lee, S., Courchet, V., Liou, D.Y., Aizawa, S., and Polleux, F. (2013). Terminal axon branching is regulated by the LKB1-NUAK1 kinase pathway via presynaptic mitochondrial capture. Cell *153*, 1510–1525.
5. Spillane, M., Ketschek, A., Merianda, T.T., Twiss, J.L., and Gallo, G. (2013). Mitochondria coordinate sites of axon branching through localized intra-axonal protein synthesis. Cell Rep. *5*, 1564–1575.
6. Wang, X., Winter, D., Ashrafi, G., Schlehe, J., Wong, Y.L., Selkoe, D., Rice, S., Steen, J., LaVoie, M.J., and Schwarz, T.L. (2011). PINK1 and Parkin target Miro for phosphorylation and degradation to arrest mitochondrial motility. Cell *147*, 893–906.
7. Brickley, K., and Stephenson, F.A. (2011). Trafficking kinesin protein (TRAK)-mediated transport of mitochondria in axons of hippocampal neurons. J. Biol. Chem. *286*, 18079–18092.
8. Wang, X., and Schwarz, T.L. (2009). The mechanism of Ca2+-dependent regulation of kinesin-mediated mitochondrial motility. Cell *136*, 163–174.
9. Vossel, K.A., Zhang, K., Brodbeck, J., Daub, A.C., Sharma, P., Finkbeiner, S., Cui, B., and Mucke, L. (2010). Tau reduction prevents Abeta-induced defects in axonal transport. Science *330*, 198.
10. Obashi, K., and Okabe, S. (2013). Regulation of mitochondrial dynamics and distribution by synapse position and neuronal activity in the axon. Eur. J. Neurosci. *38*, 2350–2363.
11. Ashrafi, G., Schlehe, J.S., LaVoie, M.J., and Schwarz, T.L. (2014). Mitophagy of damaged mitochondria occurs locally in distal neuronal axons and requires PINK1 and Parkin. J. Cell Biol. *206*, 655–670.
12. Maday, S., and Holzbaur, E.L. (2014). Autophagosome biogenesis in primary neurons follows an ordered and spatially regulated pathway. Dev. Cell *30*, 71–85.
13. Maday, S., Wallace, K.E., and Holzbaur, E.L. (2012). Autophagosomes initiate distally and mature during transport toward the cell soma in primary neurons. J. Cell Biol. *196*, 407–417.
14. Verburg, J., and Hollenbeck, P.J. (2008). Mitochondrial membrane potential in axons increases with local nerve growth factor or semaphorin signaling. J. Neurosci. *28*, 8306–8315.
15. Gazit, N., Vertkin, I., Shapira, I., Helm, M., Slomowitz, E., Sheiba, M., Mor, Y., Rizzoli, S., and Slutsky, I. (2016). IGF-1 receptor differentially regulates spontaneous and evoked transmission via mitochondria at hippocampal synapses. Neuron *89*, 583–597.
16. Kwon, S.K., Sando, R., 3rd, Lewis, T.L., Hirabayashi, Y., Maximov, A., and Polleux, F. (2016). LKB1 regulates mitochondria-dependent presynaptic calcium clearance and neurotransmitter release properties at excitatory synapses along cortical axons. PLoS Biol. *14*, e1002516.
17. Chang, K.T., Niescier, R.F., and Min, K.T. (2011). Mitochondrial matrix Ca2+ as an intrinsic signal regulating mitochondrial motility in axons. Proc. Natl. Acad. Sci. USA *108*, 15456–15461.
18. MacAskill, A.F., Brickley, K., Stephenson, F.A., and Kittler, J.T. (2009). GTPase dependent recruitment of Grif-1 by Miro1 regulates mitochondrial trafficking in hippocampal neurons. Mol. Cell. Neurosci. *40*, 301–312.

19. Saotome, M., Safiulina, D., Szabadkai, G., Das, S., Fransson, A., Aspenstrom, P., Rizzuto, R., and Hajnóczky, G. (2008). Bidirectional Ca2+-dependent control of mitochondrial dynamics by the Miro GTPase. Proc. Natl. Acad. Sci. USA *105*, 20728–20733.

20. Owens, G.C., and Walcott, E.C. (2012). Extensive fusion of mitochondria in spinal cord motor neurons. PLoS ONE *7*, e38435.

21. McKinney, S.A., Murphy, C.S., Hazelwood, K.L., Davidson, M.W., and Looger, L.L. (2009). A bright and photostable photoconvertible fluorescent protein. Nat. Methods *6*, 131–133.

22. Polleux, F., Giger, R.J., Ginty, D.D., Kolodkin, A.L., and Ghosh, A. (1998). Patterning of cortical efferent projections by semaphorin-neuropilin interactions. Science *282*, 1904–1906.

23. Polleux, F., Morrow, T., and Ghosh, A. (2000). Semaphorin 3A is a chemoattractant for cortical apical dendrites. Nature *404*, 567–573.

24. Kaifosh, P., Lovett-Barron, M., Turi, G.F., Reardon, T.R., and Losonczy, A. (2013). Septo-hippocampal GABAergic signaling across multiple modalities in awake mice. Nat. Neurosci. *16*, 1182–1184.

25. Hara, K., and Harris, R.A. (2002). The anesthetic mechanism of urethane: the effects on neurotransmitter-gated ion channels. Anesth. Analg. *94*, 313–318.

26. Zaugg, M., Lucchinetti, E., Spahn, D.R., Pasch, T., Garcia, C., and Schaub, M.C. (2002). Differential effects of anesthetics on mitochondrial K(ATP) channel activity and cardiomyocyte protection. Anesthesiology *97*, 15–23.

27. de Oliveira, L., Fraga, D.B., De Luca, R.D., Canever, L., Ghedim, F.V., Matos, M.P., Streck, E.L., Quevedo, J., and Zugno, A.I. (2011). Behavioral changes and mitochondrial dysfunction in a rat model of schizophrenia induced by ketamine. Metab. Brain Dis. *26*, 69–77.

28. Sanchez, V., Feinstein, S.D., Lunardi, N., Joksovic, P.M., Boscolo, A., Todorovic, S.M., and Jevtovic-Todorovic, V. (2011). General anesthesia causes long-term impairment of mitochondrial morphogenesis and synaptic transmission in developing rat brain. Anesthesiology *115*, 992–1002.

29. Misgeld, T., Kerschensteiner, M., Bareyre, F.M., Burgess, R.W., and Lichtman, J.W. (2007). Imaging axonal transport of mitochondria in vivo. Nat. Methods *4*, 559–561.

30. Plucińska, G., Paquet, D., Hruscha, A., Godinho, L., Haass, C., Schmid, B., and Misgeld, T. (2012). In vivo imaging of disease-related mitochondrial dynamics in a vertebrate model system. J. Neurosci. *32*, 16203–16212.

31. Sajic, M., Mastrolia, V., Lee, C.Y., Trigo, D., Sadeghian, M., Mosley, A.J., Gregson, N.A., Duchen, M.R., and Smith, K.J. (2013). Impulse conduction increases mitochondrial transport in adult mammalian peripheral nerves in vivo. PLoS Biol. *11*, e1001754.

32. Sorbara, C.D., Wagner, N.E., Ladwig, A., Nikić, I., Merkler, D., Kleele, T., Marinković, P., Naumann, R., Godinho, L., Bareyre, F.M., et al. (2014). Pervasive axonal transport deficits in multiple sclerosis models. Neuron *84*, 1183–1190.

33. Kang, J.S., Tian, J.H., Pan, P.Y., Zald, P., Li, C., Deng, C., and Sheng, Z.H. (2008). Docking of axonal mitochondria by syntaphilin controls their mobility and affects short-term facilitation. Cell *132*, 137–148.

34. Ohno, N., Kidd, G.J., Mahad, D., Kiryu-Seo, S., Avishai, A., Komuro, H., and Trapp, B.D. (2011). Myelination and axonal electrical activity modulate the distribution and motility of mitochondria at CNS nodes of Ranvier. J. Neurosci. *31*, 7249–7258.

35. Takihara, Y., Inatani, M., Eto, K., Inoue, T., Kreymerman, A., Miyake, S., Ueno, S., Nagaya, M., Nakanishi, A., Iwao, K., et al. (2015). In vivo imaging of axonal transport of mitochondria in the diseased and aged mammalian CNS. Proc. Natl. Acad. Sci. USA *112*, 10515–10520.

36. Jackson, J.G., O'Donnell, J.C., Takano, H., Coulter, D.A., and Robinson, M.B. (2014). Neuronal activity and glutamate uptake decrease mitochondrial mobility in astrocytes and position mitochondria near glutamate transporters. J. Neurosci. *34*, 1613–1624.

37. Faits, M.C., Zhang, C., Soto, F., and Kerschensteiner, D. (2016). Dendritic mitochondria reach stable positions during circuit development. eLife *5*, e11583.

38. Shidara, Y., and Hollenbeck, P.J. (2010). Defects in mitochondrial axonal transport and membrane potential without increased reactive oxygen species production in a Drosophila model of Friedreich ataxia. J. Neurosci. *30*, 11369–11378.

Current Biology, Volume *26*

Supplemental Information

Progressive Decrease of Mitochondrial Motility during Maturation of Cortical Axons In Vitro and In Vivo

Tommy L. Lewis, Jr., Gergely F. Turi, Seok-Kyu Kwon, Attila Losonczy, and Franck Polleux

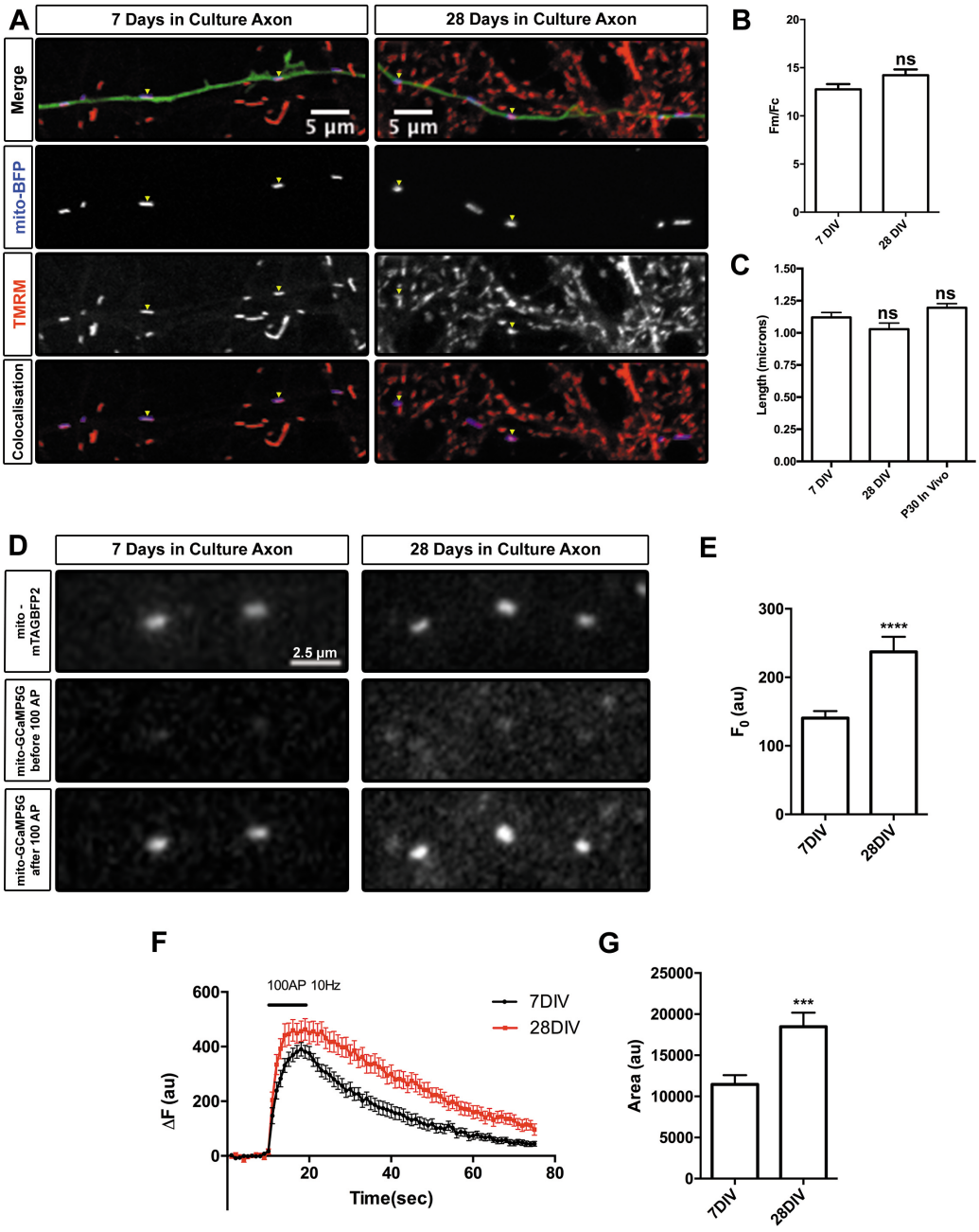
A
7 Days in Culture Axon
28 Days in Culture Axon
Merge
mito-BFP
TMRM
Colocalisation
5 µm
5 µm
B
Fm/Fc
ns
7 DIV
28 DIV
C
Length (microns)
ns
ns
7 DIV
28 DIV
P30 In Vivo
D
7 Days in Culture Axon
28 Days in Culture Axon
mito - mTAGBFP2
mito-GCaMP5G before 100 AP
mito-GCaMP5G after 100 AP
2.5 µm
E
F0 (au)
****
7DIV
28DIV
F
100AP 10Hz
7DIV
28DIV
ΔF (au)
Time(sec)
G
Area (au)
***
7DIV
28DIV

Supplemental Figure 1: Functional properties of mitochondria in immature and mature axons (Related to Figure 1 and Figure 2)

(**A**) Imaging of mitochondrial membrane potential in 7DIV and 28DIV cortical axons in culture. (Top three panels) Representative images of ex utero electroporated cortical axons labeled with cytoplasmic Venus (green), mito-mTAGBFP2 (blue, 2nd panels from the top), as well as all mitochondria with a membrane potential from all cell types via 20nM TMRM (red, 3rd panels from the top). (Bottom panels) The colocalisation threshold tool in Fiji/ImageJ was used to create overlapping pixel maps from the mito-mTAGBFP2 (blue) and TMRM (red) image panels above. Overlapping pixels are shown in purple and demonstrate that mito-mTAGBFP2 labeled mitochondria load with TMRM and therefore have a membrane potential. Yellow arrowheads mark a few mitochondria across all panels. (**B**) Quantitation of the ratio of TMRM fluorescence in mitochondria versus the cytoplasm for each labeled mitochondria in the 7 and 28DIV axons in culture. There is no significant difference between the ratio at 7 vs. 28DIV, revealing there is no difference in mitochondrial membrane potential in immature versus mature axons. N= 82 or 191 mitochondria from 6 or 8 axons for 7 or 28DIV respectively. Mann-Whitney p= 0.7630, Mean ± SEM (**C**) Mitochondrial length was measured across multiple live imaging conditions. There is no significant change in length in any of the conditions suggesting that the imaging parameters are not harming the mitochondria. N= 146, 168 or 149 mitochondria from 12, 13 or 10 axons for 7, 28DIV or P30 *in vivo* respectively. One way ANOVA p= 0.1765, Mean ± SEM (**D**) (Top panels) Axonal mitochondrial labeled with mito-mTAGBFP2 via ex utero electroporation at E15.5 and cultured to 7DIV or 28DIV. (Middle panels) Matrix calcium visualized with mito-GCaMP5G before stimulation (F_0) at 7DIV or 28DIV. (Bottom panels) Matrix calcium visualized with mito-GCaMP5G after stimulation with 100AP at 7DIV or 28DIV. (**E**) Matrix calcium is elevated in resting mitochondria from mature axons compared to resting mitochondria in immature axons. Mann-Whitney p= <0.0001, Mean ± SEM. (**F**) Time course of mitochondrial calcium uptake into the matrix upon stimulation with 100AP for 7DIV axons and 28DIV axons, Plotted as ΔF, Mean ± SEM. (**G**) Quantitation of the area under the curves in (F) showing an increase in the amount of mitochondrial Ca^{2+} import upon stimulation. N= 16 or 18 axons for 7 or 28DIV respectively. Mann-Whitney p= <0.0005, Mean ± SEM. Results E-G suggest that mitochondria in mature axons experience higher levels of calcium but are still able to respond to neuronal activity.

Study	System	PNS or CNS	Neurons imaged	Compartment	Stage/Age	Anesthesia	% Stationary Mitochondria	Measurement of Motility
Obashi and Okabe 2013	Mouse - culture	CNS	Hippocampal	Axon	19-21 DIV	N/A	~ 95% over 180 mins	-
Current Study	Mouse - culture	CNS	Cortical L2/3	Axon	21-28 DIV	N/A	98 ± 4% over 30mins, 68 ± 25% over 12hours	-
Misgeld et al 2007	Mouse - in vivo	PNS	Sciatic nerve	Axon	?	Yes - ?	~ 87% over 5 mins	> 9 mito/min
Plucinska et al 2012	Zebrafish - in vivo	PNS	Rohon-Beard	Axon	2-3 dpf	No - ?	99% distal, 83% proximal over 10 mins	~ .8 mito/min
Sajic et al 2013	Mouse - in vivo	PNS	Saphenous nerve	Axon	8-12 weeks	Yes - terminal urethane	-	~ 1 mito/axon in niave/sham
Sorbata et al 2014	Mouse - in vivo	PNS	Spinal Cord	Axon	6-12 weeks	Yes - ketamine/xylazine	93 ± 6% over 5 - 15 mins	~ .8 mito/min
Takihara et al 2015	Mouse - in vivo	CNS	Retinal Ganglion Cells	Axon	2-25 months	Yes - ketamine/xylazine	-	~ 10 mito/100µm axon/3 mins
Current Study	Mouse - in vivo	CNS	Cortical L2/3	Axon	P30/45 awake	No	93 ± 4.5% over 10 - 20 mins	~ 1 mito/axon
Misgeld et al 2007	Mouse - explant	PNS	Sciatic nerve	Axon	?	N/A	87 ± 1% over 5 mins	9 ±.3/min
Ohno et al 2011	Mouse - slice culture	CNS	Purkinje Cell	Axon	P8-9	N/A	-	~1 mito/5min
Jackson et al 2014	Rat - slice culture	CNS	Hippocampal	Dendrites	P6-12	N/A	~60% over 15 mins	-
Faits et al 2016	Mouse - retina whole mount	CNS	Retinal Ganglion Cells	Dendrites	P9-P21	N/A	~70% at P9, ~100% at P21 over 35 mins	-

Supplemental Table 1: Comparison of mitochondrial motility in mature cultures, slice cultures and *in vivo* (Related to Figure 1 and Figure 4)

Measurements of motility and/or the percentage of stationary mitochondria are compared across multiple publications that imaged mitochondrial dynamics under many different conditions and in many different neuronal types. The table demonstrates that in most studies, control/wildtype neurons show limited mitochondrial motility in mature neurons.

Supplemental Experimental Procedures

Animals

All animals were handled according to protocols approved by the Institutional Animal Care and Use Committee (IACUC) at Columbia University. Time-pregnant CD1 females were purchased from Charles Rivers. Timed-pregnant hybrid F1 females were obtained by mating inbred 129/SvJ females, and C57Bl/6J males in house [S1].

***In utero* cortical electroporation**

In utero electroporations were performed as detailed in [S1] with the exception that CD1 mice were used. Plasmids concentrations were 1μg/μl for pCAG mito-YFP and pCAG tdTomato.

Primary cortical culture and *ex utero* electroporationCortices from E15.5 CD1 mouse embryos were dissected in Hank's Buffered Salt Solution (HBSS) supplemented with Hepes (2.5 mM), $CaCl_2$ (1 mM, Sigma), $MgSO_4$ (1 mM, Sigma), $NaHCO_3$ (4mM, Sigma) and D-glucose (30 mM, Sigma), hereafter referred to as cHBSS. Cortices were dissociated in cHBSS containing papain (Worthington) and DNAse I (100 μg/ml, Sigma) for 20 min at 37°C, washed three times and manually triturated in cHBSS supplemented with DNAse. Cells were then plated at 7.5 x 10^4 cells per 35mm glass bottom dish (Mattek) coated with poly-D-lysine (1 mg/ml, Sigma) and cultured for 3-28 days in neurobasal medium supplemented with B27 (1X), FBS (2.5%), L-glutamine (2 mM). One third of the medium was changed every 5 days thereafter with non-FBS containing medium. *Ex utero* electroporation was performed as previously published in [S1].

Constructs

pCAG VGLUT1-venus, pCAG mVenus and pCAG mito-DsRED1 were previously described in [S1]. pCAG mito-YFP was created by placing the DNA encoding YFP-mito (from pYFP-Mito; Clontech) 3' to the CAG promoter using PCR. pCAG mito-mTAGBFP2 was created by placing the DNA encoding mTAGBFP2 (from the Addgene plasmid #34632) 3' to the CAG promoter and a matrix mitochondrial targeting sequence (from cytochrome C subunit VIII) using PCR. pCAG-tdTomato and pCAG-mTAGBFP were created by cloning the DNA encoding tdTomato (Clontech) or mTAGBFP (Evrogen) 3' to the CAG promoter using PCR. pCAG mEmerald-LAMP1 was created by cloning the DNA encoding LAMP1-mEmerald from mEmerald-Lysosomes-20 (from the Michael Davidson collection (Addgene plasmid #54149)) 3' to the CAG promoter by PCR. pCAG mito-mEos2 was created by cloning the DNA encoding mEos2 (from the Michael Davidson collection (Addgene plasmid #54510)) 3' to the CAG promoter and the mitochondrial targeting sequence described above via PCR. pCAG mCardinal was created by cloning the DNA encoding mCardinal (from the Michael Davidson collection (Addgene plasmid #54590) 3' to the CAG promoter using PCR. pCAG mito-GCaMP5G was created by cloning the DNA encoding GCaMP5G (from Addgene plasmid #31788) 3' to the CAG promoter and mitochondrial targeting sequence described above using PCR.

Dual color time-lapse imaging of cultured neurons

Imaging was performed between 3-28DIV in cHBSS with a 60x (1.4NA) oil objective on a Nikon Ti-e inverted microscope equipped with a Lumencor Spectra-x light engine and Andor iXon Ultra 897 EM-CCD camera. A custom quad-band excitation/mirror/emission cube (based off Chroma, 89400) followed by clean up filters (Chroma, ET525/50, ET600/50, ET435/26) were used for excitation and emission. Live imaging was done in a Tokai Hit chamber system with the following settings: top heater – 37°C, Bottom heater - 40°C, Bath heater - 37°C, Objective heater - 37°C, CO_2 – 125 mL/min of 5% CO_2, 21.4% O_2, 73.6% N_2. Videos were acquired at 0.1 fps for 30 minutes with mitochondria and presynaptic sites while videos were acquired at 2 fps for 3 minutes with lysosomes and mitochondria. Dual channel kymographs were created in NIS Elements by drawing a line along the imaged axon shaft. These kymographs were then analyzed for mitochondrial, lysosomal and VGLUT1 dynamics using NIS Elements. The Colocalisation Threshold program in FUJI/ImageJ was used to create overlapping pixel maps.

Mito-mEos2 photo-conversion and imaging

Imaging was performed on 28-30DIV distal axons of cortical neurons in cHBSS with a 40x (.95NA) air objective at 1.5x zoom on a Nikon Ti-e inverted microscope equipped with a Nikon A1 confocal. Live imaging was done in a Tokai Hit chamber with the same settings as above. Videos were acquired once every 15 minutes for 12 hours following photo-conversion of a small section of the distal axon (30 to 50 micrometers). All imaging acquisition was performed with NIS Elements and photo-conversion was done with the A1 Stimulation module. Settings for stimulation were determined experimentally based on the expression level of mEos2. Settings were 4% laser power (405nm, Coherent, 100mW) and 24 seconds stimulation of the selected region of interest. The stimulation cycle was repeated one more time on some

bright samples to photo-convert as much green mEos2 as possible (maximum of 48 seconds 405nM exposure). Mitochondrial morphology was not affected by this stimulation protocol. For confocal microscopy imaging sessions, we had 15 μW of power through the objective (40X, 0.95NA), the objective was properly filled for diffraction limited imaging, and the area of the focal spot was on the order of ~0.31 μm^2. Under these illumination conditions, using published absorption cross sections for YFP, a given fluorophore residing at the focus of the light would be excited every ~2x10^-7 seconds meaning under continuous illumination over 98% of the time the fluorophore would not be excited. Semi-automated tracking was performed on photo-converted mitochondria using the NIS Elements tracking module.

TMRM and mito-aGCaMP5G imaging

TMRM (Life Technologies) 10 mM stock was diluted in cHBSS to 10μM. Neuron cultures were then loaded with 20nM TMRM in cHBSS for 20 minutes at 37C. After 20 minutes, the medium was replaced with cHBSS containing 5nM TMRM for the imaging session. Live imaging was performed as above with the 60x objective on the confocal microscope. The Colocalisation Threshold program in Fiji/ImageJ was used to create overlapping pixel maps. For mitochondrial Ca^{2+} imaging, we used modified normal tyrode solution which contained (in mM): 145 NaCl, 2.5 KCl, 10 HEPES pH7.4, 2 $CaCl_2$,1 $MgCl_2$,10 glucose. For blocking spontaneous activity, APV (50μM, Tocris) and CNQX (20μM, Tocris) was added. Action potentials were triggered by 1ms current injections with a concentric bipolar electrode (FHC) placed 20μm away from labeled axons. We applied 100APs at 10Hz with 20V using the stimulator (Model 2100, A-M systems) and imaged with 1s interval during 90sec. Images were analyzed in Fiji (Image J) using a Time Series Analyzer (v3.0) plugin. Mito-GCaMP5G signal and nearby backgrounds were selected by circular ROIs and intensities were measured by the plug-in. After intensities were corrected for background subtraction, ΔF values were calculated from (F-F0). F0 values were defined by averaging 10 frames before stimulation.

Surgery

To image mitochondrial motility *in vivo* we implanted mice with a cranial window above the somatosensory cortex contralaterally to the electroporated hemisphere. First the mice were anesthetized with isoflurane and treated with buprenorphine (0.1 mg/kg, subcutaneous) to minimize post-operative discomfort. We then exposed the skull and drilled a slightly smaller than 3-mm diameter circle centered over the somatosensory cortex. We removed the bone and dura, and irrigated the tissue with sterile chilled cortex buffer (125 mM NaCl, 5 mM KCl, 10 mM glucose, 10 mM HEPES, 2 mM CaCl2 and 2 mM MgCl2) to stop any sporadic bleeding. A sterilized glass coverslip (3 mm diameter) was placed over the craniotomy and secured to the bone with tissue adhesive (Vetbond, 3M). Finally, a stainless steel headpost was attached to the posterior part of the skull with dental acrylic (Unifast Trad; GC America Inc. IL USA). We monitored the mice every 12 hours for three days after surgery, administering buprenorphine to minimize any signs of discomfort. For acute imaging (P10-12) we anaesthetized the mice with a cocktail of ketamine – xylazine (i.p. 80 and 5 mg/kg body weight for ketamine and xylazine respectively) then performed the surgery described above. During the imaging session the depth of the anesthesia was checked regularly by pinching the mice's hind leg and anesthetics was applied in case of any sign of muscle contraction. For awake imaging (P30-45), after the three day recovery period mice were hand habituated followed by head restraint on a freely moving treadmill for increasing amounts of time for at least three more days before the first imaging session. Mice imaged awake at P30 had a minimum of six days recovery before the first imaging session while mice imaged at P45 had at least twenty one days of recovery before the first imaging session.

***In vivo* 2-photon microscopy imaging**

We use an *in vivo* resonant galvo-based multi-photon microscopy system (Bruker) and an ultra-fast pulsed laser beam (Chameleon, Coherent; tuned to 920-nm wavelength, average 20-40mW out of the objective) controlled with an electro-optical modulator to excite mito-YFP and tdTomato through a 20X or 40X objective (Nikon). Distilled water served to connect the water immersion objective with the window. Green and red fluorescence were separated with an emission filter cube set (green, HQ525/70m-2p; red, HQ607/45m-2p; 575dcxr). Fluorescent light was detected with photomultiplier tubes (green GFP fluorescence, GaAsP PMT; red tdTomato fluorescence, multi-alkali PMT) operated with PrairieView software. Once mice were head-fixed, we used goniometers (Edmund Optics) to adjust the angle of the mouse's head up to 10 degrees to make the imaging window parallel to the objective. Timelapse image series were collected in red (tdTomato signal) and green (mito-YFP signal) channels by acquiring 30 frames at 0.1 Hz for 10 – 15 minutes. We can estimate the level of two-photon excitation following the prescriptions given in Denk et al, 1990 [S3] combined with the known parameters of our laser and

microscope, and the 2-P cross section of YFP at 920nm. Under these conditions, any given fluorophore in the focus of the beam has a less than 10% chance of being excited per laser pulse. We are still very far from saturation conditions, and direct non-linear damage is highly unlikely. Per scan the total energy delivered into the diffraction limited spot is on the order of 6nJ, and most of that is not absorbed, so local heating is also insignificant. Time-series were motion-corrected based on the static tdTomato signal as described in [S2] and the same displacements were applied to the green channel.

Statistics

All statistical analysis was performed in GraphPad Prism 6. Statistical tests used are labeled in the figure legends. Graphs were created in GraphPad Prism 6 or Microscoft Excel.

Supplemental References

S1. Courchet, J., Lewis, T.L., Jr., Lee, S., Courchet, V., Liou, D.Y., Aizawa, S., and Polleux, F. (2013). Terminal axon branching is regulated by the LKB1-NUAK1 kinase pathway via presynaptic mitochondrial capture. Cell *153*, 1510-1525.

S2. Kaifosh, P., Lovett-Barron, M., Turi, G.F., Reardon, T.R., and Losonczy, A. (2013). Septo-hippocampal GABAergic signaling across multiple modalities in awake mice. Nat Neurosci *16*, 1182-1184.

S3. Denk, W., Strickler, J.H., and Web, W.W. (1990). Two-photon laser scanning fluorescence microscopy. Science *248*, 73-76.